SRTTU

JCARME
ISSN: 2228-7922
Journal of Computational and Applied Research in Mechanical Engineering
Vol. 9, No. 1, pp. 141-152
jcarme.sru.ac.ir

Identification of rotor bearing parameters using vibration response data in a turbocharger rotor

Rajasekhara Reddy Mutra* **and J. Srinivas**

Department of Mechanical Engineering, National Institute of Technology, Rourkela, Odisha,769008, India

Article info:
Received: 12/12/2017
Accepted: 24/10/2018
Online: 27/10/2018

Keywords:
Turbocharger,
Diagnostic techniques,
Hilbert transforms,
Bearing forces,
Frequency response,
RBF Network.

Abstract
Turbochargers are most widely used in automotive, marine and locomotive applications with diesel engines. To increase the engine performance nowadays, in aerospace applications also turbochargers are used. Mostly the turbocharger rotors are supported over the fluid film bearings. With the operation, lubricant properties continuously alter leading to different load bearing capacities. This paper deals with the diagnostic approach for prediction of shaft unbalance and the bearing parameters using the measured frequency responses at the bearing locations. After validating the natural frequencies of the rotor finite element model with experimental analysis, the response histories of the rotor are recorded. The influence of the parameters such as bearing clearance, oil viscosity and casing stiffness on the unbalance response is studied. By considering three levels each for shaft unbalance and oil viscosity, the output data in terms of four statistical parameters of equivalent Hilbert envelopes in the frequency domain are measured. The data are inversely trained using Radial Basis Function (RBF) neural network model to predict the unbalance and oil viscosity indices from given output response characteristics. The outputs of the RBF model are validated thoroughly. This approach finds changes in the rotor bearing parameters from the measured responses in a dynamic manner. The results indicate that there is an appreciable effect of lubricant viscosity at two different temperatures compared to other parameters within the operating speed range. The identification methodology using the neural network is quite fast and reliable

1. Introduction

Today most of the diesel engines are equipped with turbochargers. In principle, turbocharger works on a closed cycle, which receives expanded hot burnt exhaust gases at the turbine wheel's to allow its compressor wheel to pressurize the atmospheric air required for engine combustion. Due to its relatively smaller sizes, often its speeds are of order 100-300 krpm. If proper maintenance is not followed, it may hamper the usual operation of the entire engine. Sometimes the unburnt gases/fuel particles coming out of the engine may result in improper expansion on the turbine of the turbocharger forming pitting and corrosion defects in blades. Therefore, the turbocharger rotors have time to time unbalance and bearing faults due to

*Corresponding author
Email address: rajmech03@gmail.com

surrounding high-temperature conditions. The small malfunctioning at high speeds of operation amplifies the changes in vibration signals. The schematic of the turbocharger rotor is shown in the Fig. 1 with input and outputs from the engine.

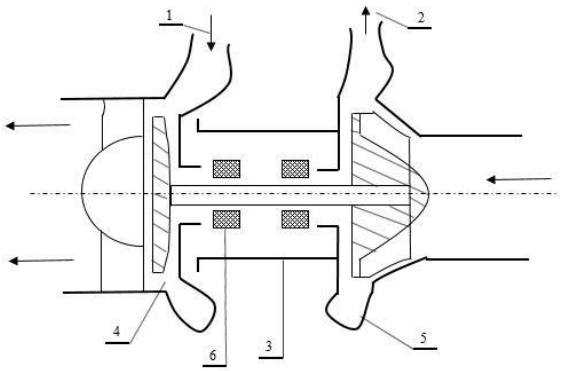

Fig. 1. Turbocharger sketch; 1.Exhaust channel of the engine, 2.Intake duck of engine, 3.Turbocharger bearing housing, 4. Turbine, 5.Compressor, 6.Journal bearings.

To predict the accurate performance and emission in the engine, the turbocharger simulations are very important. Sakellaridis et al. [1] described the performance of the turbocharger and parameters of the closed cycle with a variation of the load and validated the predictions with the experimental test. Kozhenkov and Deitch [2] presented an application of the developed procedure to model the dynamics of high-velocity turbocharger's rotor system. Some previous works [3–5] explain the stability analysis and manufacturing tolerance clearances on the dynamic characteristics of the turbochargers, which were placed in the engines. Gjika et al. [6] explained the prediction of the lateral dynamic response of the rotor-bearing system in the turbocharger and validated this with the test data obtained from the large speed turbocharger. Some of the literature [7, 8] present the experimental and theoretical methodologies to obtain the mechanical and frictional losses in the automotive turbocharger model. Wang et al. [9] proposed an algorithm to identify the bearing coefficients, and residual unbalances of the rotor based on the unbalance response by using the Rayleigh method. Yao et al. [10] described the modal expansion technique for the identification and optimization of the rotor-bearing system. This method allows for identifying the axial unbalance and its phase and magnitude.

Various sound and vibration based diagnostic approaches are available for monitoring the engine condition. Von Flotow [11] explained the basic measurement techniques, along with damage signatures with the sensors, for health monitoring of blade and disk. Holzenkamp et al. [12] explained the data-driven processing and signal-monitoring techniques to classify the seed fault imposed on the compressor ring bearing in the turbocharger. Pantelelis et al. [13] proposed a method to find the automatic fault diagnosis of the engine by creating a turbocharger model using finite element method. The complete faults of the system were predicted from neural networks. Machado et al. [14] proposed a method to predict the faults parameters in real systems with the use of response measurements. Chandra and Sekhar [15] identified the speed dependent damping and natural frequencies of the multi-degree rotor-bearing system with the wavelet-based method. Vencl and Rac [16] explained the most of the bearing failures due to the different parameters such as surface fatigue, adhesive, and abrasive, and also explained wear types in the bearing materials. Machado and Cavalca [17] described the numerical model to analyze the influence of wear on the dynamic response of the rotor-bearing system in the frequency domain. Chatterton et al. [18] proposed a method to know the effect of the electrical pitting on the static behavior of the bearing. Barelli et al. [19] developed a diagnostic procedure, specifically for the turbochargers, installed on the internal combustion engines. Serrano et al. [20] explained the procedure to identify the turbocharger rotor precession movement in an automobile application. This technique was based on infrared light diode sensors. Some recent studies [21, 22] conducted experimental analysis on the turbocharger rotor bearing system to investigate the thermos hydrodynamic performance and operational characteristics of the turbine. Novotny et al. [23] experimentally verified the numerical computational model of the turbocharger of a diesel engine for transient analysis with the inclusion of influence of oil and structure

temperature changes. They also explained the dynamic analysis of a turbocharger rotor bearing system under different conditions. The influence of unbalances and bearing parameters on the dynamics of the system is very essential. Although many studies are available in the literature, the identification of rotor bearing parameters in inverse modeling was found in a few papers.

The present work deals with some studies relating to condition monitoring of an ideal engine turbocharger rotor-bearing system. The rotor model is developed using finite element analysis and is first validated with experimental work on a prototype. Unbalance, bearing oil viscosity, bearing clearances and casing stiffness are altered, and the changes in the dynamic response are observed at different operating speeds. As a practical study in condition monitoring, the unbalance and bearing oil viscosity are predicted using the Fourier transform of the Hilbert envelopes. The statistical representative parameters of the signals in terms of Mean, Variance, Kurtosis and Skewness values are computed. In order to predict the condition measures in terms of unbalance and oil viscosity, an inversely trained neural network model is employed. After testing the model, it is used as a successful paradigm to give the state of system unbalance and bearing viscosity by simply providing the frequency response at the bearing. A test case of short bearing approximation is considered to evaluate nonlinear bearing forces.

2. Modeling based condition monitoring rotor

The dynamic model of the rotor system is analyzed as a finite element model represented by the following equations of motion:

$$[M]\{\ddot{q}\}+[[C]+\Omega[G]]\{\dot{q}\}+[K]\{q\}=\{F\} \qquad (1)$$

Here, [M], [C], [G] and [K] are respectively the assembled global mass, damping, gyroscopic and stiffness matrices of the shaft and disc elements [24]. {F} is a force vector containing unbalance, gravity and bearing forces. {q} is the displacement vector represented by bending in two planes as follows:

$$\{q\}=[u_{x_1} \quad u_{y_1} \quad \theta_{x1} \quad \theta_{y_1} \quad .... \quad \theta_{y_n} \quad]^T \qquad (2)$$

The mass and gyroscopic matrices for the disc elements can be written as:

$$[M_d]=\begin{bmatrix} m_d & & & \\ & m_d & & \\ & & J_d & \\ & & & J_d \end{bmatrix} \qquad (3)$$

$$[G_d]=\begin{bmatrix} 0 & & & \\ & 0 & & \\ & & 0 & J_p \\ & & -J_p & 0 \end{bmatrix} \qquad (4)$$

Fig. 2 shows the finite element model of the rotor system considered in the present work.

The model consists of eight elements with each element having eight degrees of freedom corresponding to bending in two planes resulting in a total of 36 degrees of freedom. Shear deformation is taken into consideration, and the discs are assumed to be rigid and lumped at respective nodes in the model. Also, the bearing is assumed as a short journal type, and the corresponding dynamic bearing forces are applied at respective bearing nodes on either side. The model considers oil film forces given by short bearing approximation. The time-varying forces together with unbalance, gravity, and gyroscopic terms are solved with the global equations of motion using fourth order Range-Kutta time marching integration scheme. The short bearing forces, considered in terms of nodal displacements and velocities, are obtained from a simplified Reynold's equation [25]. These are given by:

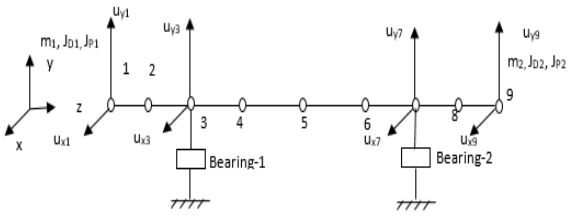

Fig. 2. Finite element model of the rotor system.

$$F_t = \frac{\mu R L^3 \varepsilon}{2C_r{}^2\left(1-\varepsilon^2\right)^2} * \left[4\dot{\varepsilon} + \frac{\pi}{2}\sqrt{1-\varepsilon^2}\left(\Omega - 2\dot{\phi}\right)\right] \quad (5)$$

$$F_r = \frac{-\mu R L^3}{2C_r{}^2\left(1-\varepsilon^2\right)^2} * \left[\frac{\pi\dot{\varepsilon}\left(1+2\varepsilon^2\right)}{\sqrt{1-\varepsilon^2}} + 2\varepsilon^2\left(\Omega - 2\dot{\phi}\right)\right] \quad (6)$$

where:

$$\varepsilon = \frac{e}{C_r}, \quad e = \sqrt{x^2 + y^2} \quad (7)$$

and, μ is the dynamic viscosity, Ω is the rotational speed, Cr is the radial clearance of the bearing, and e represents the eccentricity. The component forces in X and Y directions are given as:

$$F_x = -F_t \cos\phi - F_r \sin\phi \quad (8)$$

$$F_y = -F_r \cos\phi + F_t \sin\phi \quad (9)$$

2.1 Condition monitoring

For the system described by Eq. (1), in order to identify the states, due to variations in unbalance and bearing forces (ΔF), the motion of the system can be obtained as:

$$[M]\{\ddot{q}+\Delta\ddot{q}\} + \left[[C] + \Omega[G]\right]* \{\dot{q}+\Delta\dot{q}\} + [K]\{q+\Delta q\} = \{F+\Delta F\}$$

(or)

$$[M]\{\Delta\ddot{q}\} + \left[[C] + \Omega[G]\right]\{\Delta\dot{q}\} + [K]\{\Delta q\} = \{\Delta F\} \quad (10)$$

3. Numerical studies

The reliability of the model is first validated with experimental analysis. After validation of the model, it is employed to generate the signals at different unbalance conditions in the discs and the bearing force variations due to the oil film at different oil viscosities.

In fact, the unbalance in the compressor (left) is due to the speed variation occurring because of the variations in the pressure of expanded gases on the turbine due to insufficient combustion. Similarly, a variation of the bearing forces may be due to inadequate maintenance of bearing fluid. The flowchart of the methodology is shown in Fig. 3.

As it is not possible to conduct experiments by inducing the faults in the test rig for safety reasons, simulated experimental data is derived from the finite element model. Based on the parametric studies the frequency responses are distinguished using statistical data. Further, the data are used to estimate the corresponding unbalance and bearing oil viscosities by means of the trained neural network model.

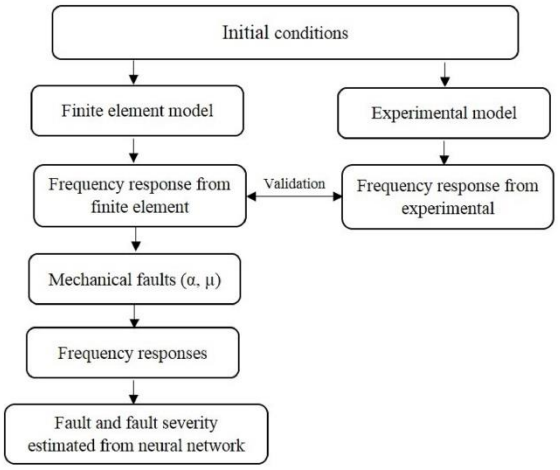

Fig. 3. Flowchart of the methodology.

3.1. Validation of the model (Experimental)

The prototype used for experimental work is shown in the Fig. 4, where a dual disk rotor is placed on the two oil-film bearings. The motor is connected to the shaft with the help of a jaw-coupler. To measure the output signals two accelerometers (PG 109 Mo, frequency range 1 to 10,000 Hz) are placed in two lateral directions on each bearing. Using a digital storage oscilloscope (model- DPO 43034) the output signals are observed.

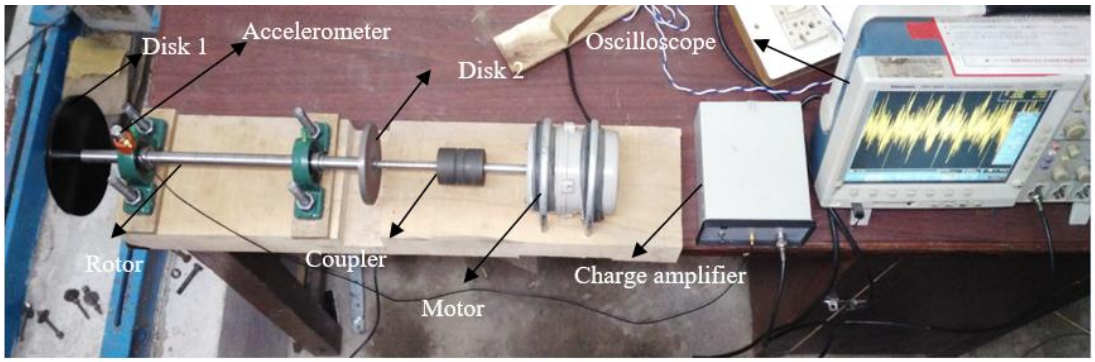

Fig. 4. Rotor model used for experimental work.

Table 1 shows the data of the rotor system which are used in the experimental work.

From the experimental data and using the Hilbert transformation method the time envelope and Fast Fourier Transform (FFT) are plotted at the left bearing at a rotor speed of 900 rpm. Fig. 5 shows the time history and FFT plots obtained from the experimental data at the left bearing in X-direction.

Fig. 6 shows the frequency response at the left bearing node obtained from the finite element model with the same input data. It is observed that the fundamental frequencies obtained from the experimental and finite element model are close to each other, and this model now can be used to carry out the parametric studies.

Table 1. System data for experimental work

Properties	Value
Left disc mass (m_{d1} (kg))	1.4
Right disc mass (m_{d2} (kg))	1
Rotor diameter (d_{sh} (m))	0.016
Rotor length (m)	0.48
Left disc diameter moment of inertia (I_{d1} (kgm^2))	6.3×10^{-4}
Right disc diameter moment of inertia (I_{d2} (kgm^2))	4.5×10^{-4}
Left disc polar moment of inertia (J_{d1} (kgm^2))	1.2×10^{-3}
Right disc polar moment of inertia (J_{d2} (kgm^2))	9×10^{-4}
Rotor material density (kg/m^3)	7800
Young's modulus (E (GPa))	200
Initial lubricant viscosity (Pa-s)	265.7×10^{-4}
Distance between the bearings (m)	0.22
Distance from disc1 to left bearing	0.09
Distance from disc2 to right bearing	0.09

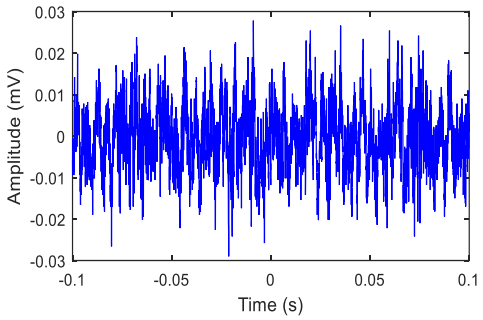

(a)

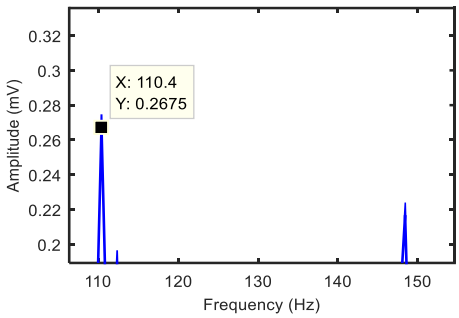

(b)

Fig. 5. Experimental results; (a) time history at left bearing and (b) frequency response at left bearing.

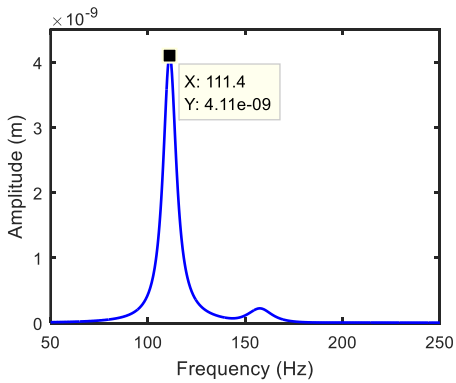

Fig. 6. Frequency response at left bearing from finite element method.

3.2. Parametric studies

The various signal processing methods such as FFT, Hilbert Transform (HT),Wavelet Transform (WT) and Short Time Fourier Transform (STFT) have been utilized to analyze vibration signals to diagnose the condition of the system. Some limitations such as mother wavelet selection and level/scale play a major role in capturing the inherent features in wavelet analysis. Recently, other time-frequency analysis methods named HT and Hilbert–Huang Transform (HHT) have become more and more popular because of their better time-frequency resolution. Continuous Wavelet Transform (CWT) requires proper selection of scale, while HT is applicable only to the mono-component signal.

In the present work, the difference in the responses for each fault cases are amplified using FFT and HT. Finally, based on the fault studies, the type and severity of the fault are estimated using neural network models.

In the field of signal theory, HT is one of the most important operators. Either by the direct method using the FFT or Kronig-Kramers relations using an analytical signal theory the HT is computed numerically. HT can be applied on a single frequency response function which is measured using a single excitation level. HT can be used to create an analytic signal from a real signal. The $\pm\pi/2$ phase-shift operator is the basic property of HT. Thus, the HT of a real signal:

$f(t)=\cos(\omega_0 t)$ is given by $\hat{f}(t)=\sin(\omega_0 t)$.

Together they form an analytic signal where the instantaneous amplitude is expressed as[26]:

$$A(t)=\sqrt{f^2(t)+\hat{f}^2(t)}=\sqrt{\begin{matrix}cso^2(\omega_0 t)+\\ \sin^2(\omega_0 t)\end{matrix}}=1 \qquad (11)$$

The instantaneous frequency can be obtained from the phase:

$$\varphi(t)=arctan\left(\frac{\hat{f}(t)}{f(t)}\right)=\omega_0 t \qquad (12)$$

where $\omega_0=\omega(t)$. Healthy and faulty vibration signal are found to be associated with unique predominant frequency components and unique instantaneous amplitudes. These frequencies and amplitude information can be used for the detection of common faults, such as a broken rotor bar, unbalanced rotor, bowed rotor, bearing defect, voltage unbalance and stator faults. Fig. 7 shows the Campbell diagram for the rotor system. The critical speed is found to be at 3000, 8000, 20000, 32000 and 38000 rpm approximately

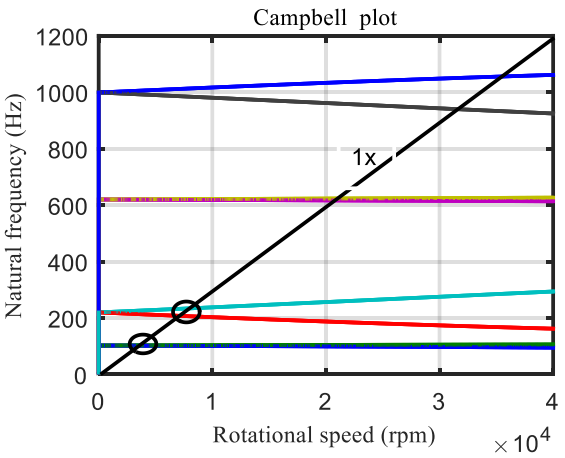

Fig. 7. Campbell diagram.

The rotor unbalance is considered through increasing unbalance at the left disc node. The generalized mathematical expression for altering the unbalance is taken as $m_{d1}e_1=(\alpha\times m_d\times e)$. Here, α is increasing unbalance factor, which is greater than or equal to 1. The bearing force variations are due to changes in the clearance and oil film viscosities (μ). The viscosity of the oil depends on the operating temperature. Here the temperature ranges are taken from 40^0 C to 90^0 C [27]. The effect of the unbalance and variation of the oil viscosities on the dynamics of the rotor system is illustrated at different speeds. Fig. 8 shows the frequency response plots at the different values of the α and μ at a rotor speed of 20,000 rpm.

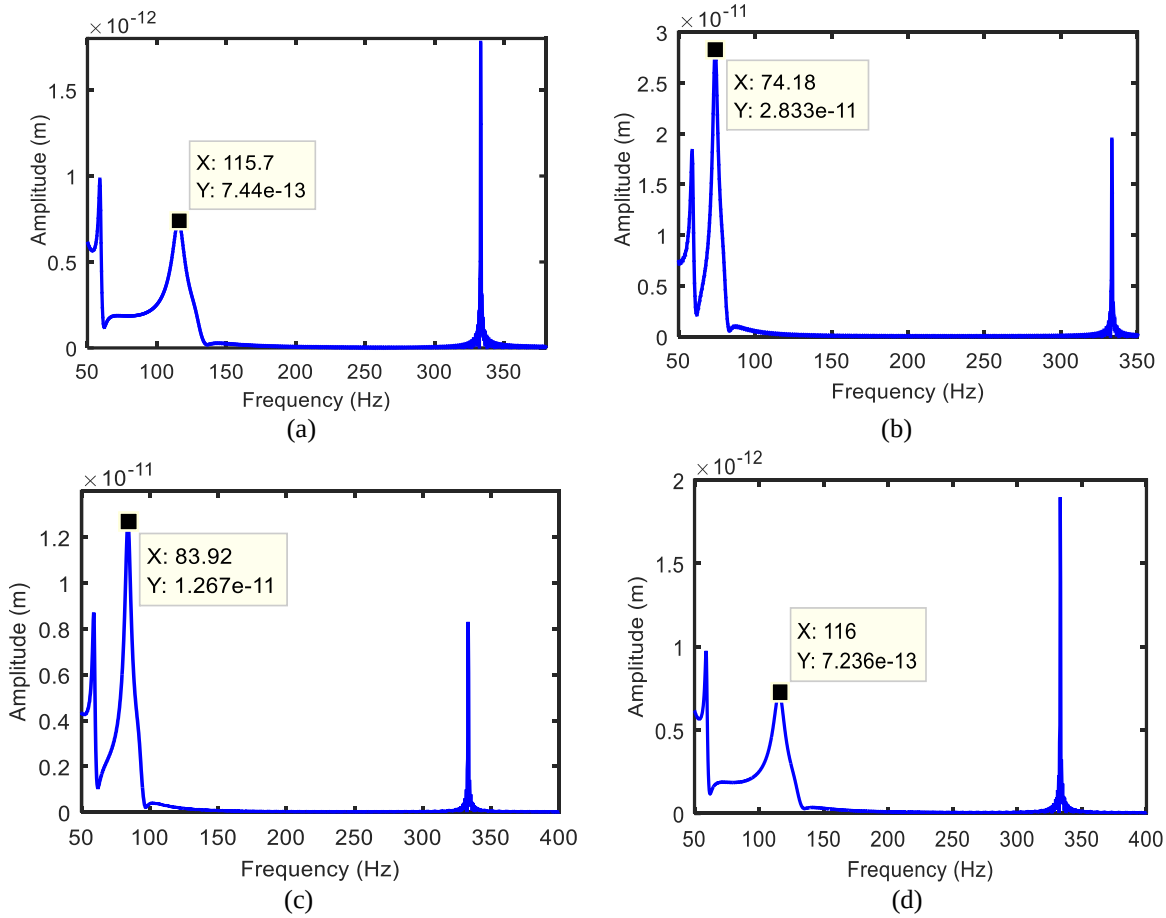

Fig. 8. Frequency response at the left bearing node at rotor speed (Ω)=20000 rpm; (a) α =1.2, μ=145.8e-4 Pa-s, (b) α=2 ,μ=145.8e-4 Pa-s, (c) α=1.6, μ=145.8 e-4 Pa-s, and (d) α=1.6 μ=910.5 e-4 Pa-s.

It is observed that when the increase of the unbalance instability of the system occurs, the change in the oil dynamic viscosity also influences the stability of the rotor system. And it is also noted that due to consideration of the unbalance and variation of the oil dynamic viscosity the multiple peaks in frequency response represents an unstable condition of the rotor.

Fig. 9 shows the frequency response of the system at different values of the bearing clearance at a rotor speed of 20000 rpm. Here, the unbalance and viscosity are considered as α=1.2, μ=265.7×10^{-4} Pa-s.

It is observed that as the bearing clearance increases the amplitude of the system increases slightly, but it does not influence the dynamics of the system much. Fig. 10 shows the frequency response of the system with different bearing casing stiffnesses (K_c) at a rotor speed of 10000 rpm. It is observed that as the bearing casing stiffness increases, the sub-synchronous amplitude reduces slightly. From all the above studies, the dynamics of the rotor system is much influenced by the unbalance and viscosity of the lubricant. So in inverse modeling, these two parameters are only considered.

In order to identify each frequency domain response, four statistical parameters are considered. These are Mean, Variance, Kurtosis, and Skewness [28]. Even two FFT plots are identical, there is a marked difference between the four statistical parameters. The first central moment or Mean is shown in Eq. (13). In practice, the Mean is estimated by the average, expressed in Eq. (14).

$$\mu = E(Z) = E(\bar{Z}) \tag{13}$$

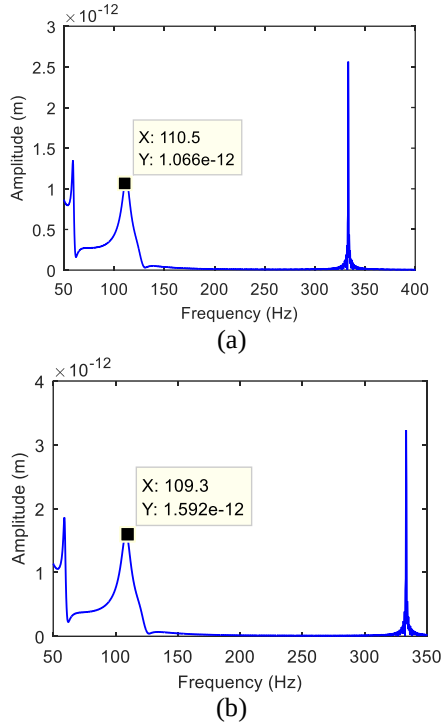

Fig. 9. Frequency response at the left bearing node for different bearing clearances; (a) C=200×10^{-6} m and (b) C=500×10^{-6} m.

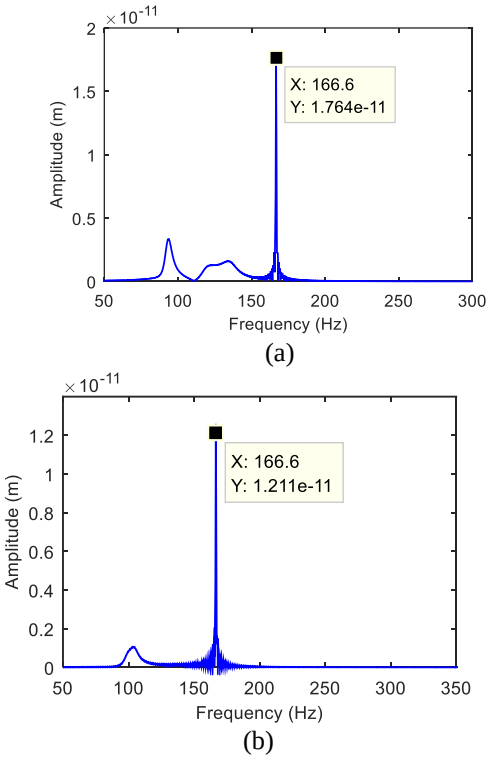

Fig. 10. Frequency response at the left bearing node for different bearing casing stiffness; (a) K_c=1×10^6 N/m and (b) K_c=1×10^7 N/m.

Estimated by:

$$\bar{Z} = \frac{1}{M}\sum_{i=1}^{M} Z_i. \tag{14}$$

The variance or second central moment is given in Eq. (15) along with its estimator in Eq. (16). The standard deviation is shown in Eq. (17).

$$V = E(Z-\mu)^2 \tag{15}$$

Estimated by:

$$\bar{V} = \frac{1}{M-1}\sum_{i=1}^{M}(Z_i - \bar{Z})^2 \tag{16}$$

$$\sigma = \sqrt{V} \tag{17}$$

The Skewness or the third central moment is given in Eq. (18), and its estimator is shown in the Eq. (19).

$$s = \frac{E(Z-\mu)^3}{\sigma^3} \tag{18}$$

$$\hat{s} = \frac{m\sum(z-\mu)^3}{(m-1)(m-2)\sigma^3} \tag{19}$$

The fourth central moment, Kurtosis, and its estimator are shown in Eqs. (20 and 21), respectively.

$$k = \frac{E(Z-\mu)^4}{\sigma^4} - 3 \tag{20}$$

$$\hat{k} = \frac{m(m+1)\sum(z-\mu)^4 - \frac{3(m-1)}{m}\sigma^4}{(m-1)(m-2)(m-3)\sigma^4} \tag{21}$$

where *m* is the sample size.

The variation of statistical parameters, respect to temperature, is shown in Fig. 11. As the temperature changes, the viscosity of the lubricant also changes. Further viscosity variation influences the dynamics of the system. It is observed that as the temperature increases the Mean and Variance of the response also rise, whereas Kurtosis and Skewness reduce. Table 2 shows the set of these statistical parameters calculated by parametric studies.

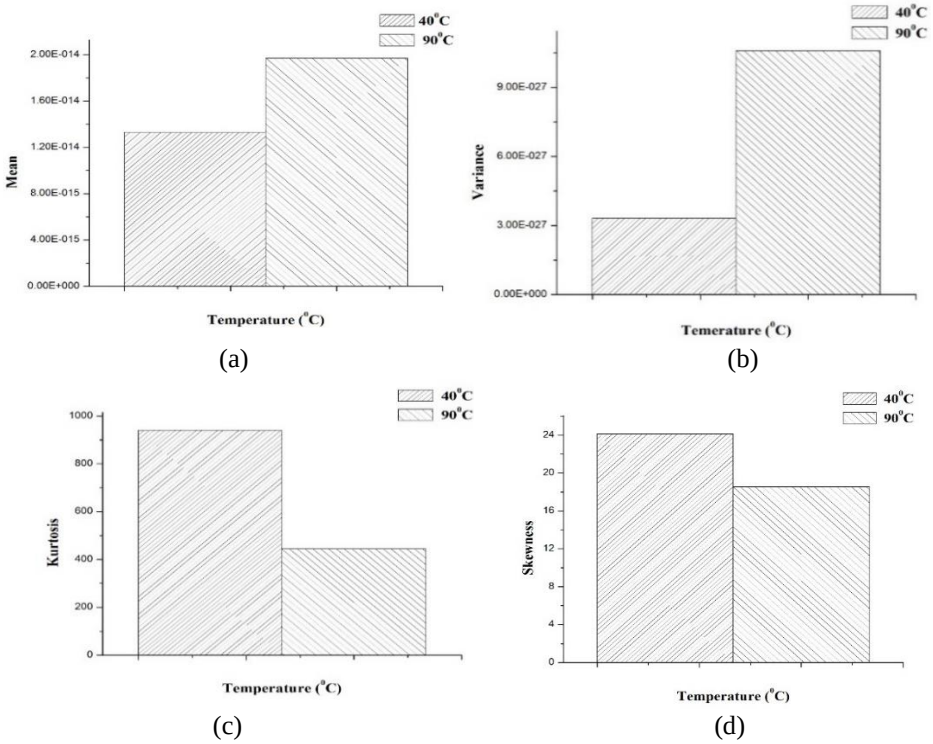

Fig. 11. Variation of statistical parameters at different temperature values; (a) Mean, (b) Variance, (c) Kotosis, and (d) Skewness.

Table 2. Central moments data for different values of α and μ.

Sl. no	α	μ	(Ω)=10000 rpm				(Ω)=20000 rpm			
		(Pa-s) $\times 10^{-4}$	Mean $\times 10^{-15}$	Variance $\times 10^{-27}$	Kurtosis $\times 10^{3}$	Skewness	Mean $\times 10^{-14}$	Variance $\times 10^{-25}$	Kurtosis $\times 10^{3}$	Skewness
1	1.2	910.5	5.54	3.31	0.94	24.138	2.538	1.315	1.731	37.220
2	1.2	265.7	5.49	3.29	0.917	23.88	2.524	1.269	1.670	36.551
3	1.2	145.8	10.14	10.61	0.443	18.52	2.385	1.04	1.386	33.326
4	1.6	910.5	8.75	16.9	5.22	63.69	2.552	1.315	1.732	37.230
5	1.6	265.7	8.72	17.1	5.24	63.71	2.53	1.27	1.67	36.563
6	1.6	145.8	14.0	33.3	3.77	51.40	2.37	1.012	1.33	32.74
7	2	910.5	13.3	57.4	6.30	72.68	2.63	1.32	1.710	36.92
8	2	265.7	13.3	57.9	6.30	72.69	2.61	1.28	1.64	36.25
9	2	145.8	19.7	100.6	5.69	67.649	2.73	1.31	1.11	29.763

3.3 Inverse model development

Fig. 12 shows the input and output of the proposed radial basis function network model for the prediction of the unbalance attenuation and bearing oil dynamic viscosity. Radial basis functions are embedded into a two-layer feed-forward neural network. Set of iputs and outputs is characterized by such a network. There is a layer, processed between the inputs and outputs, is represented as hidden units. The RBF network function is expressed as:

$$y\left(\frac{t}{\theta}\right) = G\left(\frac{x[t]}{\theta}\right) = w_0 + \sum_{n=1}^{N} w_n \exp\left(\frac{[x[t]-\mu]^2}{2\sigma_n^2}\right) \quad (22)$$

Table 3. Results of identification.

Sl. no	Mean $\times 10^{-14}$	Variance $\times 10^{-26}$	Kurtosis $\times 10^{3}$	Skewness	Output parameters					
					α predicted		α_{act}	$\mu_{predicted}$ (Pa-s) $\times 10^{-4}$		$\mu_{act} \times 10^{-4}$ (Pa-s)
					RBF	BP		RBF	BP	
1	2.18	9.24	1.588	18.61	1.05	0.93	1.0	449	437	455
2	2.45	6.63	1.73	24.19	1.58	1.75	1.6	640	649	637

Network parameter:

$$\theta = \{w_j\}_j \cup \{\mu_j\}_j \cup \{\sigma_j\}_j \quad (23)$$

In the present work, the network is used to predict the faulty factors. A training data, consisting of the central moment data such as Mean, Variance, Kurtosis, and Skewness as the inputs, and the corresponding faulty factors (α, μ) are employed as the outputs to train an RBF Network. Details of training can be found in the open literature [29].

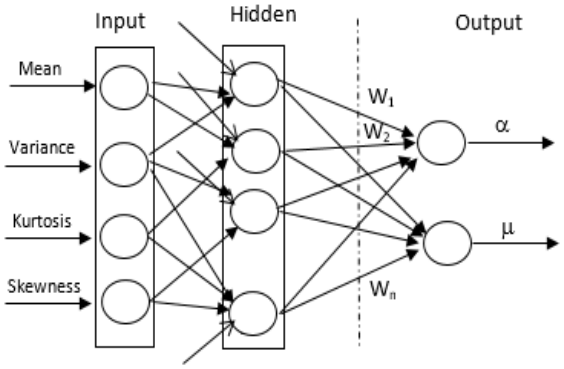

Fig. 12. The architecture of radial basis function network.

The convergence trend, with nine hidden nodes, is shown in Fig. 13. There is no much more difference in the mean square error between inputs and outputs with increasing the hidden nodes.

The test data containing two situations of the available targets are shown in Table 3. The results predicted by the RBF and three-layer backpropagation (BP) network are compared with the measured values. It is seen that the deviation between predicted and actual values of α and μ is less than two percent in both cases, but RBF has more effectiveness with limited parameters required during training.

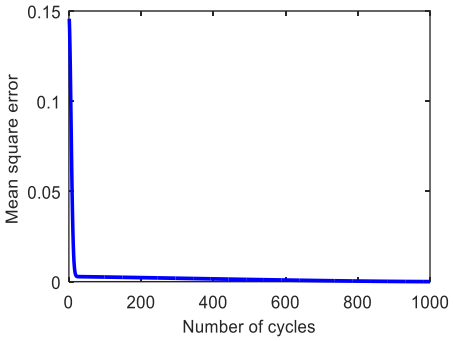

Fig. 13. Trend of convergency.

4. Conclusions

In the present work, the dynamic modeling and fault identification of the rotor-bearing system of the turbocharger is presented. A dual-disk rotor is analyzed by finite element modeling, and the faults are simulated with unbalance response. After validation with the experimental work, the central moment data (Mean, Variance, Kurtosis, and Skewness) are recorded for various fault conditions. A training data containing the central moments as the inputs and corresponding fault factors as the output is employed to train the RBF network. The results of the identification of two test cases are reported. It was found that the deviation between the predicted and actual data is less than 3%. The present neural network model can be extended for obtaining the bearing wear parameters along with multiple other faults. Further, the trained neural network model may be employed as a function estimator for an optimum design problem of the faulty system.

References

[1] N. F. Sakellaridis, S.I. Raptotasios, A.K. Antonopoulos, G.C. Mavropoulos, D.T. Hountalas, "Development and validation of a new turbocharger

simulation methodology for marine two stroke diesel engine modelling and diagnostic applications", *Energy*. Vol. 91, No. 1, pp. 952-966 (2015).

[2] A. A. Kozhenkov, R.S. Deitch, 'Three-Dimensional Finite Element Simulation of Nonlinear Dynamic Rotor Systems of a Turbocharger", *J. Vib. Acoust*. Vol. 130, No. 3, pp. 031003-8, (2008).

[3] Hao Zhang, Zhanqun Shi, Shunxin Zhang, Fengshou Gu, Andrew Ball, "Stability analysis for a turbocharger rotor system under nonlinear hydrodynamic forces", *Research and Essay*. Vol. 8, No. 1, pp. 1495-1511, (2013).

[4] L. Wang, G. Bin, X. Li, X. Zhang, "Effects of floating ring bearing manufacturing tolerance clearances on the dynamic characteristics for turbocharger", *Chin. J. Mech. Eng*, Vol. 28, No. 3, pp. 530-540, (2015).

[5] B. Schweizer, "Dynamics and stability of turbocharger rotors", *Arch Appl Mech*, Vol. 80, No. 9, pp. 1017-1043, (2009).

[6] K. Gjika, L. San Andrés, G. D. Larue, "Nonlinear Dynamic Behavior of Turbocharger Rotor-Bearing Systems with Hydrodynamic Oil Film and Squeeze Film Damper in Series: Prediction and Experiment", *J. Comput. Nonlinear Dyn*, Vol. 5, No. 4, pp. 041006-8, (2010).

[7] J. R. Serrano, P. Olmeda, A. Tiseira, L. M. García-Cuevas, A. Lefebvre, "Theoretical and experimental study of mechanical losses in automotive turbochargers", *Energy*, Vol. 55, No. 1, pp. 888-898, (2013).

[8] M. Deligant, P. Podevin, G. Descombes, "Experimental identification of turbocharger mechanical friction losses, Energy". Vol. 39, No. 1, pp. 388-394, (2012).

[9] A. Wang, W. Yao, K. He, G. Meng, X. Cheng, J. Yang, "Analytical modelling and numerical experiment for simultaneous identification of unbalance and rolling-bearing coefficients of the continuous single-disc and single-span rotor-bearing system with Rayleigh beam model", *Mech. Syst. Signal Process.*, Vol. 116, No. 1, pp. 322-346, (2019).

[10] J. Yao, L. Liu, F. Yang, F. Scarpa, J. Gao, "Identification and optimization of unbalance parameters in rotor-bearing systems", *J. Sound Vib.*, Vol. 431, No. 1, pp. 54-69, (2018).

[11] A. Von Flotow, M. Mercadal, P. Tappert, "Health monitoring and prognostics of blades and disks with blade tip sensors", "*IEEE Aerosp. Conf. Proc.*", Montana, USA, Vol. 6, pp. 433-440, (2000).

[12] M. Holzenkamp, J. R. Kolodziej, S. Boedo, S. Delmontte, "Seeded Fault Testing and Classification of Dynamically Loaded Floating Ring Compressor Bearings", *ASCE-ASME J. Risk Uncertain. Eng. Syst. Part B Mech. Eng*, Vol. 2, No. 2, pp. 021003-1, (2016).

[13] N. G. Pantelelis, A. E. Kanarachos, N. Gotzias, "Neural networks and simple models for the fault diagnosis of naval turbochargers", *Math. Comput. Simul*, Vol. 51, No. 3-4, pp. 387-397, (2000).

[14] T. H. Machado, R. U. Mendes, K. L. Cavalca, "Directional frequency response applied to wear identification in hydrodynamic bearings", *Mech. Res. Commun*, Vol. 74, No. 1, pp.60-71, (2016).

[15] N. H. Chandra, A. S. Sekhar, "Wavelet transform based estimation of modal parameters of rotors during operation", *Measurement*, Vol. 130, No. 1, pp. 264-278, (2018).

[16] A. Vencl, A. Rac, "Diesel engine crankshaft journal bearings failures: Case study, *Eng. Fail. Anal.*, Vol. 44, No. 1, pp. 217-228, (2014).

[17] T. H. Machado, and K. L. Cavalca, "Modeling of hydrodynamic bearing wear in rotor-bearing systems", *Mech. Res. Commun*, Vol. 69, No. 1, pp. 15-23, (2015).

[18] S. Chatterton, P. Pennacchi, A. Vania, "Electrical pitting of tilting-pad thrust bearings: Modelling and experimental evidence", *Tribol. Int*. Vol. 103, No. 1, pp. 475-486, (2016).

[19] L. Barelli, G. Bidini, F. Bonucci, "Diagnosis methodology for the turbocharger groups installed on a 1 MW internal combustion engine", *Appl. Energy*. Vol. 86, No. 12, pp. 2721-2730, (2009).

[20] J. R. Serrano, C. Guardiola, V. Dolz, M. A. López, F. Bouffaud, "Study of the turbocharger shaft motion by means of infrared sensors", *Mech. Syst. Signal Process*. Vol. 56-57, No. 1, pp. 246-258, (2015).

[21] Y. Li, F. Liang, Y. Zhou, S. Ding, F. Du, M. Zhou, J. Bi, Y. Cai, "Numerical and experimental investigation on thermohydrodynamic performance of turbocharger rotor-bearing system", *Appl. Therm. Eng.* Vol. 121, No. 5, pp. 27-38, (2017).

[22] L. Shao, J. Zhu, X. Meng, X. Wei, X. Ma, "Experimental study of an organic Rankine cycle system with radial inflow turbine and R123", *Appl. Therm. Eng*. Vol. 124, No. 1, pp. 940-947, (2017).

[23] P. Novotný, P. Škara, J. Hliník, "The effective computational model of the hydrodynamics Journal floating ring bearing for Simulations of long transient regimes of turbocharger rotor dynamics", *Int. J. Mech. Sci*. Vol. 148, No. 1, pp. 611-619, (2018).

[24] W. Li, Y. Yang, D. Sheng, J. Chen, "A novel nonlinear model of rotor/bearing/seal system and numerical analysis", *Mech. Mach. Theory*. Vol. 46, No. 5, pp. 618-631, (2011).

[25] M. Dakel, S. Baguet, R. Dufour, "Nonlinear dynamics of a support-excited flexible rotor with hydrodynamic journal bearings", *J. Sound Vib*, Vol. 333, No. 10, pp. 2774-2799, (2014).

[26] P. Konar, and P. Chattopadhyay, "Multi-class fault diagnosis of induction motor using Hilbert and Wavelet Transform", *Appl. Soft Comput*. Vol. 30, No. 1, pp. 341-352, (2015).

[27] Viscopedia A free encyclopedia for viscosity. http://www.viscopedia.com/ (accessed September 20, 2016).

[28] S. G. Mattson, and S. M. Pandit, "Statistical moments of autoregressive model residuals for damage localisation, *Mech. Syst. Signal Process*, Vol. 20, No. 3, pp.627-645, (2006).

[29] R. Rojas, *Neural Networks*, Springer Berlin Heidelberg, Berlin, Heidelberg, (1996).

How to cite this paper:

Rajasekhara Reddy Mutra and J. Srinivas," Identification of rotor bearing parameters using vibration response data in a turbocharger rotor" *Journal of Computational and Applied Research in Mechanical Engineering*, Vol. 9, No. 1, pp. 141-152, (2019).

DOI: 10.22061/jcarme.2018.3165.1347

URL: http://jcarme.sru.ac.ir/?_action=showPDF&article=901